Talanta 83 (2010) 233–240

Contents lists available at ScienceDirect

Talanta

journal homepage: www.elsevier.com/locate/talanta

Direct determination of benzo[*a*]pyrene in water samples by a gold nanoparticle-based solid phase extraction method and laser-excited time-resolved Shpol'skii spectrometry

Huiyong Wang, Andres D. Campiglia*

Department of Chemistry, P.O. Box 25000, University of Central Florida, Orlando, FL 32816-2366, USA

ARTICLE INFO

Article history:
Received 17 July 2010
Received in revised form 8 September 2010
Accepted 8 September 2010
Available online 16 September 2010

Keywords:
Polycyclic aromatic hydrocarbons
Solid-phase extraction
Gold nanoparticles
Shpol'skii spectroscopy

ABSTRACT

The strong affinity between polycyclic aromatic hydrocarbons (PAH) and the surface of gold colloids is investigated to device an extraction method for water samples. Within the 20–100 nm particle diameter range, the 20 nm gold nanoparticles showed the best extraction efficiencies for all the studied analytes. The new approach is combined to laser-excited time-resolved Shpol'skii spectrometry for the direct analysis of benzo[*a*]pyrene in drinking water samples. For a 500 μL sample volume, the analytical figures of merit demonstrate precise and accurate analysis at the parts-per-trillion level. The extraction efficiencies are statistically equivalent to 100% with relative standard deviations lower than 2%. The average recoveries were varied from 87.5% to 96.5% for different concentration of analytes. The simplicity of the experimental procedure, the low analysis cost, and the excellent analytical figures of merit demonstrate the potential of this approach for routine analysis of drinking water samples.

1. Introduction

The fact that several polycyclic aromatic hydrocarbons (PAH) can induce cancer has been documented in numerous epidemiological studies [1]. Their omnipresence in the environment—which results from incomplete combustion of organic materials involved in countless natural processes or human activities—makes them a permanent threat to human health. The Environmental Protection Agency (EPA) lists 16 PAH as "Consent Decree" priority pollutants [2]. Benzo[*a*]pyrene (B[*a*]P) is the most carcinogenic PAH on the EPA list and its concentration alone is often used as a measure of risk [3]. Because a primary route of potential human exposure to PAH is the ingestion of contaminated drinking water, the EPA recommends the routine monitoring of water samples taken from municipal wells.

The EPA "Maximum Contaminant Level" (MCL) for B[*a*]P in drinking water is 0.2 ng mL^{-1} [3]. This low concentration often challenges classical methodology. The general approach consists of sample pre-concentration and chromatographic analysis. Solid phase extraction (SPE) is nowadays the preferred method to preconcentrate PAH. Typically, 1 L of water is processed through an extraction membrane in approximately 1 h. This volume of water is recommended to reach detectable concentrations by chromatographic techniques [2]. Gas chromatography (GC) and high-performance liquid chromatography (HPLC) are the basis for standard PAH identification and determination [4–13]. Because the entire procedure, i.e. PAH extraction and chromatographic analysis, takes about 2 h/sample, the development of rapid screening techniques is still under the scope.

This article builds upon significant improvements we have introduced recently to Shpol'skii spectroscopy [14,15]. This technique has long been recognized for its unique capability of providing efficient and adequate resolution of individual PAH at the concentration ratios found in environmental samples without previous chromatographic separation [16]. Our approach, which we have named laser excited time-resolved Shpol'skii spectrometry (LETRSS), eliminates the complications of traditional methodology for 77K and 4.2K measurements with the aid of a cryogenic fiber-optic probe. PAH determination is carried out with an instrumental system specifically designed for the efficient collection of wavelength time matrices (WTM) and time-resolved excitation–emission matrices (TREEM) [17,18]. These multidimensional data formats combine spectral and lifetime information for the unambiguous determination of target PAH. WTM consist of a series of successive emission spectra collected during the time domain of the fluorescence decay. Adding the temporal dimension to fluorescence spectra reports on spectral peak purity for accurate PAH determination in highly complex matrixes. TREEM, which compound a series of excitation–emission matrices recorded at several delays after the excitation pulse, provide the best time window for minimum spectral overlapping. In comparison to HPLC,

* Corresponding author. Tel.: +1 517 432 1141; fax: +1 517 432 3855.
E-mail addresses: chwanghy@hotmail.com (H. Wang), acampigl@mail.ucf.edu (A.D. Campiglia).

0039-9140/$ – see front matter © 2010 Elsevier B.V. All rights reserved.
doi:10.1016/j.talanta.2010.09.013

the main advantages of LETRSS include shorter analysis time (~15 min/sample), reduced solvent consumption (100 μL/sample) and lower limits of detection (LOD). Depending on the PAH, LETRSS-LOD are one to two order of magnitude better than HPLC-LOD [19–21].

But the research presented here tackles a different aspect as it focuses on the extraction of PAH from water samples. The new approach, which we have named solid phase nano-extraction, is based on the adsorption of PAH on the surface of gold nanoparticles (Au NPs) [22–24]. When combined to LETRSS, the entire sample procedure consumes 100 μL of organic solvents per sample. 500 μL of water sample are sufficient to determine B[*a*]P at picogram concentration level (0.5×10^{-12} g) or femtomol (1.8×10^{-15}) level. The precision of measurements at the parts-per-trillion level is outstanding. The accuracy of analysis is excellent as well.

2. Experimental

2.1. Chemicals and reagents

All solvents were Aldrich HPLC grade. Unless otherwise noted, Nanopure water was used throughout. All chemicals were analytical reagent grade and used without further purification. Gold colloids were purchased from Ted Pella, Inc. and used as received. anthracene, phenanthrene, fluoranthene, pyrene, chrysene, B[*a*]P, benzo[*b*]fluoranthene, benzo[*g,h,i*]perylene and indeno[*1,2,3-cd*]pyrene were acquired from Accustandard at their highest purity available. Rhodamine 610 was acquired from Exciton and was used with the tunable dye laser according to specifications.

Note: Use extreme caution when handling PAH known to be extremely toxic.

2.2. Instrumentation

Sample mixing was carried out with a Maxi Mix III Rotary Shaker (Type M65800, Barnstead-Thermolyne) equipped with a PT500X6A Vortex Mixer accessory. Centrifugation was performed with a MiniSpin centrifuge (Eppendorf) with maximum rotational speed of 13,400 rotations per minute (rpm).

Absorbance measurements were carried out with a single-beam spectrophotometer (model Cary 50, Varian) equipped with a 75-W pulsed xenon lamp, 2 nm fixed band-pass, and 24,000 nm min^{-1} maximum scan rate.

Steady-state excitation and fluorescence spectra and signal intensities were recorded from un-degassed solutions using a commercial spectrofluorimeter (Photon Technology International). The excitation source was a continuous-wave 75 W pulsed Xenon lamp with broadband illumination from 200 to 2000 nm. The excitation and the emission monochromators had the same reciprocal linear dispersion (4 nm mm^{-1}) and accuracy (±1 nm with 0.25 nm resolution). The gratings (1200 grooves mm^{-1}) were blazed at 300 and 400 nm, respectively. Detection was made with a photomultiplier tube (PMT, model 1527) with spectral response from 185 to 650 nm. The instrument was computer-controlled using commercial software (Felix32) specifically designed for the system.

2.3. 4.2K fluorescence spectral and lifetime analysis

The instrumentation for LETRSS was developed in house. Full reports comparing its performance to conventional approaches are available in the literature [25,26]. Sample excitation was carried out by directing the output of a Northern Lights tunable dye laser (Dakota Technologies, Inc.) through a potassium dihydrogen phosphate (KDP) frequency-doubling crystal. The dye laser was operated on Rhodamine 610, and it was pumped with the second harmonic of a 10 Hz Nd:YAG Q-switched solid-state laser (Big Sky Laser Technologies). Time-resolved fluorescence detection was made with a front-illuminated intensified charge fiber-coupled device (ICCD, Andor Technology). The minimum gate time full width at half-maximum of the intensifier was 2 ns, and the CCD active area was 690 pixels × 256 pixels (26 nm^2 pixel size photocathode). The ICCD was mounted at the exit focal plane of a spectrograph (SPEX 270 M) equipped with a grating (1200 grooves mm^{-1}) blazed at 500 nm. The system was used in the external trigger mode. The gate delay, width, and step were controlled with a digital delay generator (DG 535, Stanford Research System, Inc.) via a GPIB interface (National Instruments). Custom Labview software (National Instruments) was developed in house for complete instrumental control and data collection [15].

The cryogenic probe consisted of a fiber optic assembly with one excitation and six collection fibers fed into a 1.25-m-long section of copper tubing that provided mechanical support to lower the probe into the liquid helium. All the fibers were 3 m long and 500 μm core diameter silica-clad silica with polyimide buffer coating (Polymicro Technologies, Inc.). At the analysis end, the excitation and emission fibers were arranged in a conventional six-around-one configuration, bundled with vacuum epoxy (Torr-Seal, Varian) and fed into a metal sleeve for mechanical support. The copper tubing was flared stopping a swage nut tapped to allow for the threading of a 0.75 mL polypropylene sample vial. At the instrument end, the excitation fiber was positioned in an ST connection and aligned with the beam of the tunable dye laser while the emission fibers were bundled with vacuum epoxy in a slit configuration, fed into a metal sleeve, and aligned with the entrance slit of the spectrometer.

Fluorescence lifetimes were collected via the WTM procedure,[15,27,28] which consisted of the following three steps: (1) collection of full sample and background WTM; (2) subtraction of the background decay curve from the fluorescence decay curve at the wavelength of maximum fluorescence for each PAH; (3) fitting of the background-corrected data to single exponentials. Origin software (version 7, Microcal Software, Inc.) was used for curve fitting of fluorescence lifetimes. Fitted decay curves were obtained by fixing y_0 and x_0 at a value of zero. Otherwise noted, the agreement between the calculated and the observed points over the first two lifetimes of the decays agreed to within about 1% and the residuals showed no systematic trends.

2.4. Sample procedures

PAH standard solutions for RTF measurements were prepared in methanol–water 1% (v/v). B[*a*]P standard solutions for Shpol'skii Spectroscopy were prepared in *n*-octane. UV absorption and RTF measurements were carried out with commercial instrumentation by pouring un-degassed liquid solutions into standard (1 cm × 1 cm) quartz cuvettes. Measurements at liquid helium temperature (4.2 K) were performed with the aid of the cryogenic probe and the laser system. Sample freezing was accomplished by lowering the copper tubing into the liquid cryogen. The liquid helium was held in a Dewar with 60 L storage capacity. Such a volume of liquid helium would typically last for three weeks of daily use, averaging 15–20 samples/day. Complete sample freezing took less than 90 s. Measurements were made with the tip of the fiber optic probe ~0.5 cm above the surface of the frozen sample. The position of the probe was held constant with the screw cap of the sample cell.

Tap water samples were spiked with micro-liter volumes of B[*a*]P stock solutions in 1% methanol–water (v/v) to provide final PAH concentrations equal to 0.05, 0.1 and 0.2 ng mL^{-1}. Each water sample was examined in triplicate via the following procedure: 500 μL of water sample were mixed with 950 μL of Au NPs solution (20 nm particle diameter) in a 2 mL micro-plain glass tube. The vessel was placed in a mechanical shaker for 5 min at 1400 rpm. Centrifugation was carried out for 20 min at 13,400 rpm. The super-

natant was removed with the aid of a micro-pipette and the precipitate was successively spiked with 0.2 μL of 1-pentanethiol and 99.8 μL of *n*-octane. After 5 min of equilibration time, the layer of *n*-octane was transferred to the vessel of the cryogenic probe for 4.2 K measurements.

3. Results and discussion

3.1. Centrifugation studies on the Au NPs and PAH solutions

Quantitative extraction of PAH with Au colloids requires an appropriate centrifugation time for complete NPs precipitation. This parameter was investigated via UV–vis absorption spectroscopy for the following particle diameters: 5, 10, 20, 40, 60, 80 and 100 nm. The commercial standards were received in 100% water but working solutions were prepared in methanol–water 1% (v/v). This alcohol content was added to facilitate the complete dissolution of trace levels of PAH in the working solutions. Centrifugation was carried out in 2 mL micro-plain glass tubes at the maximum rotational speed (13,400 rpm). Absorption spectra were recorded before and after centrifugation. Centrifuged solutions presented a clear aqueous phase (supernatant) and a reddish solid phase due to the precipitation of Au NPs.

Absorption spectra from the supernatant solution were recorded at several centrifugation time intervals. The supernatant solution was removed from the micro-plain tube with a glass micro-pipette. Fig. 1 plots the absorption of the supernatant as a function of centrifugation time. Signal intensity was monitored at the maximum absorption wavelength of the Au surface plasmon resonance band, which varied between 520.3 nm (20 nm Au NPs diameter) and 566.7 nm (100 nm Au NPs diameter). 5 nm Au NPs did not precipitate at the maximum speed of our centrifuge. As shown in the figure, the expected correlation between precipitation time and particle size was observed as the larger (or heavier) Au NPs presented the shorter centrifugation times. Further studies were carried out with a 20 min centrifugation time to assure the complete precipitation of the entire diameter range of Au NPs under investigation.

The possibility of PAH adhesion to the walls of the centrifugation vessels and/or their precipitation solely due to centrifugation were investigated via RTF spectroscopy. Table 1 shows the maximum excitation and emission wavelengths ($\lambda_{exc}/\lambda_{em}$) of 8 EPA-PAH, the linear dynamic ranges of their RTF calibration curves and the statistics of the fittings. PAH centrifugation was carried out in 2 mL micro-plain glass tubes for 20 min. The initial tests were done with the upper linear concentrations of the RTF calibration curves. Their fluorescence intensities were monitored before (I_{NC}) and after centrifugation (I_C). Their average values were obtained from triplicate measurements ($N = 3$). Within a confidence interval of 95% ($\alpha = 0.05$), only pyrene, benzo[*b*]fluoranthene, benzo[*g,h,i*]perylene and indeno[*1,2,3-cd*]pyrene showed some adhesion and/or precipitation due to centrifugation. These PAH were then investigated at lower concentrations levels to find out the maximum working concentration free from adhesion and/or precipitation. The working concentration ranges are listed in Table 1 along with the statistical comparisons of the RTF signals from their most concentrated solutions.

3.2. Particle diameter effect on the extraction of PAH

Table 2 summarizes pertinent information on the preparation of extracting solutions with Au NPs varying from 20 to 100 nm diameter. The number of NPs was kept constant in all extracting solutions (5.544×10^9 particles/mL) as a tentative means of minimizing the role that collisions might play in the extraction of PAH. Four model

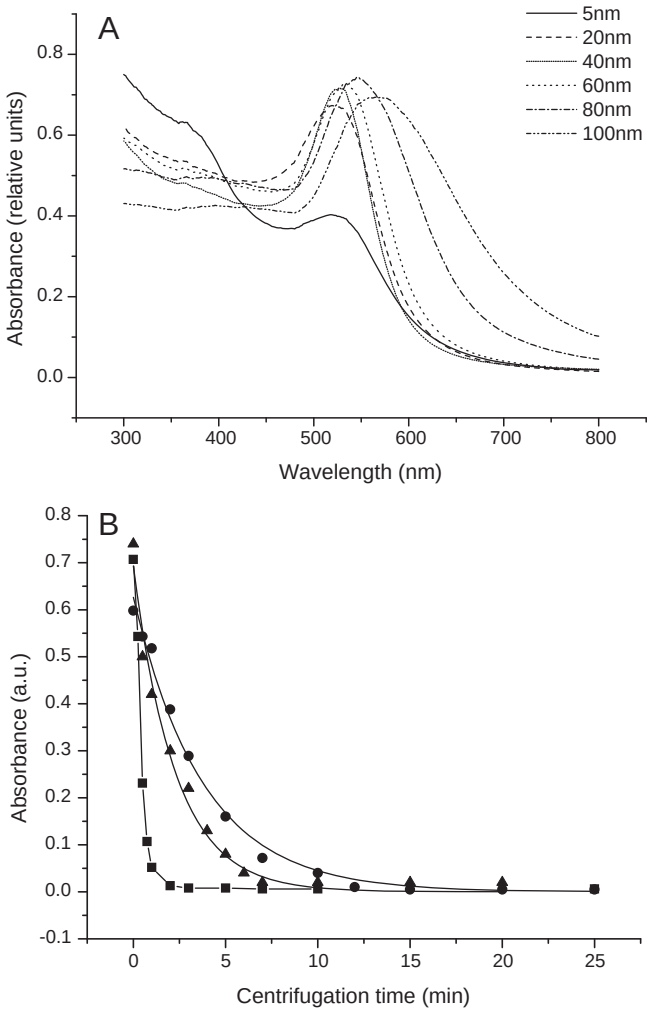

Fig. 1. Absorbance spectral of Au NPs with different diameters (A) and intensity (a. u. = arbitrary units) of Au NPs as a function of centrifugation time (B). Only the absorbance of 20 (●), 40 (▲) and 60 (■) nm particle diameters are plotted in the graph B.

PAH, namely anthracene, pyrene, B[*a*]P and indeno[*1,2,3-cd*]pyrene were selected as representative cases of EPA-PAH containing 3, 4, 5 and 6 rings, respectively. Their concentrations were kept at 10 ng mL^{-1}, i.e. within the four working concentration ranges of Table 1. All working solutions were prepared in 1% methanol–water (v/v). Prior to 20 min centrifugation, PAH and Au NPs were shaken for 5 min at 1400 rpm. The 5 min shaking time was found to be long enough to achieve maximum PAH extraction (data not shown).

The extraction efficiencies as a function of particle diameter and total surface area of Au were summarized in Table 3. Their values are based on the RTF signals of PAH solutions before and after centrifugation. The signal intensities from the supernatants, i.e. the PAH solutions after centrifugation, were measured in the absence of NPs to avoid potential fluorescence quenching. As expected, the extraction efficiencies of the four PAH increased with the particle diameter and the total surface area of Au. Because the extraction is based on the adsorption of PAH molecules on the surface of the Au NPs, the large particles can extract more PAH than small ones due to their large surface area. More interesting to note is the trend we observed for the number of extracted molecules per nm^2 of surface area of Au (see Fig. 2A). The 20 nm particles, which provide the lowest total surface area, are the "most efficient" for extracting PAH. The four decays in Fig. 2A fit the mathematical expression $y = Ax^{-n}$, where y is the number of PAH molecules extracted per

Table 1
Working concentration ranges for PAH extraction.

PAH[a]	Ex/Em (nm)	LDR (ng mL^{-1})	Calibration curve[b]	Working concentration range[c] (ng mL^{-1})	I_{NC}[d] ($\times 10^4$ counts)	I_C[e] ($\times 10^4$ counts)	t_{exp}[f]
Anthracene	251/378	5–40	$Y = 0.2071X + 0.077$ $R^2 = 0.9989$	5–40	8.26 ± 0.12	8.03 ± 0.09	2.66
Phenanthrene	294/347	5–200	$Y = 0.4994X - 0.6041$ $R^2 = 0.9994$	5–200	82.47 ± 1.23	80.14 ± 1.49	2.53
Fluoranthene	288/450	5–200	$Y = 0.9583X + 1.7071$ $R^2 = 0.9989$	5–200	163.57 ± 3.34	160.69 ± 6.48	0.68
Pyrene	334/371	5–100	$Y = 0.7795X - 0.2516$ $R^2 = 0.9967$	5–75	54.93 ± 0.7	54.35 ± 1.0	0.85
Chrysene	269/361	2–20	$Y = 0.9244X + 1.7139$ $R^2 = 0.992$	2–20	21.65 ± 0.68	20.85 ± 1.09	1.08
Benzo[*a*]pyrene	298/404	5–30	$Y = 0.1447X + 1.3759$ $R^2 = 0.9925$	5–30	5.76 ± 0.11	5.61 ± 0.09	1.83
Benzo[b]fluoranthene	300/445	5–40	$Y = 0.3323X + 0.5372$ $R^2 = 0.9985$	5–10	3.86 ± 0.08	3.71 ± 0.10	2.14
Benzo[*g,h,i*]perylene	305/420	2–20	$Y = 0.0917X + 0.545$ $R^2 = 0.9894$	2–10	1.44 ± 0.06	1.29 ± 0.08	2.60
Indeno[*1,2,3-cd*]pyrene	302/510	5–75	$Y = 0.0955X + 0.5918$ $R^2 = 0.9922$	5–30	3.34 ± 0.09	3.28 ± 0.06	0.96

[a] PAH solutions were made in 1% methanol–water (v/v).
[b] Linear regressions obtained via the least squares method.
[c] Working concentration range free from PAH precipitation.
[d] Net fluorescence intensity (blank subtracted) recorded prior to centrifugation from upper working concentration in column 5.
[e] Net fluorescence intensity recorded after centrifugation from upper working concentration in column 5.
[f] Student's *t*-test of experimental averages before (I_{NC}) and after (I_C) centrifugation. $T_{critical} = 3.18$ ($\alpha = 0.05$; $N_{NC} = N_C = 3$).

Table 2
Pertinent parameters for the preparation of working solutions of gold nanoparticles.

Diameter (nm)	Particles/mL commercial solution[a]	Surface area/particle[b] (nm^2)	TSA/mL commercial solution[c] (nm^2/mL)	Volume of commercial solution[d] (μL)	Total surface area/mL working solution[e] (nm^2/mL)
20	7.0×10^{11}	1,256.6	8.7962×10^{14}	7.92	7.0×10^{12}
40	9.0×10^{10}	5,026.5	4.5238×10^{14}	61.6	2.8×10^{13}
60	2.6×10^{10}	11,309.7	2.9405×10^{14}	213.2	6.3×10^{13}
80	1.1×10^{10}	20,106.2	2.2117×10^{14}	504.0	1.1×10^{14}
100	5.6×10^{9}	31,415.9	1.7593×10^{14}	990.0	1.7×10^{14}

[a] Information obtained from commercial supplier. All NPs solutions were purchased in water.
[b] Surface area of one particle was calculated according to the formula $4\pi r^2$, where r is the radius of the particle.
[c] Total surface area (TSA) of Au was calculated by multiplying the number of particles in 1 mL of commercial solution (column 2) to the surface area of one particle (column 3).
[d] Volume of commercial solution added to 1 mL of working solution to obtain 5.544×10^9 Au NPs per 1 mL of working solution.
[e] Total surface area of Au in each working solution was calculated according to the formula: [value in column 4] × [volume of commercial solution (μL)/1 mL of working solution]. All working solutions were prepared in 1% methanol–water (v/v).

nm^2 of surface area of Au and x is the particle diameter in nm. As shown in Fig. 2B, the values of A and n vary considerably with PAH concentration but the decays follow the same mathematical model, i.e. $y = Ax^{-n}$. The same behavior—but different A and n values—was observed for pyrene, B[*a*]P and indeno[*1,2,3-cd*]pyrene (data not shown). Based on these results we can postulate the following: (a) the number of PAH molecules that one can extract per nm^2 of surface area of Au increases with the initial concentration of PAH; and (b) within the 20–100 nm particle diameter range, the best extraction efficiencies are obtained with 20 nm Au NPs independent of initial PAH concentration and/or type of PAH. All further studies were then performed with 20 nm Au NPs.

Table 3
Efficiency of PAH extraction as a function of gold nanoparticle diameter.

Diameter (nm)	TSA[b] (10^{14} nm^2)	Anthracene[a]		Pyrene[a]		Benzo[*a*]pyrene[a]		Indeno[*1,2,3-cd*]pyrene[a]	
		Ext[c] (%)	Molecules per nm^2[d]	Ext[c] (%)	Molecules per nm^2[d]	Ext[c] (%)	Molecules per nm^2[d]	Ext[c] (%)	Molecules per nm^2[d]
20	0.070	14.3 ± 1.2	0.690	13.5 ± 0.9	0.574	12.8 ± 1.5	0.436	14.0 ± 1.0	0.436
40	0.279	26.5 ± 0.9	0.321	23.5 ± 0.6	0.251	23.1 ± 0.8	0.198	25.7 ± 0.6	0.201
60	0.627	51.2 ± 0.6	0.276	52.4 ± 0.8	0.249	45.8 ± 0.6	0.174	55.9 ± 0.5	0.194
80	1.115	67.1 ± 0.5	0.203	66.8 ± 0.5	0.178	61.6 ± 0.6	0.132	68.5 ± 0.5	0.134
100	1.742	90.6 ± 0.4	0.176	94.6 ± 1.0	0.162	87.8 ± 0.5	0.120	92.9 ± 0.4	0.116

[a] Initial PAH concentration was 10 ng mL^{-1}. All working solutions were prepared in 1% methanol–water (v/v).
[b] TSA calculated according to Table 2.
[c] Ext = PAH extraction. Reported values are the averages of three independent extractions from the same PAH solution.
[d] Average number of extracted molecules per nm^2 of surface area of Au NPs were calculated by equation: ([Initial PAH concentration] × [sample volume] × [Ext] × 6.02×10^{23})/([PAH formula weight] × 10^9 × [TSA]).

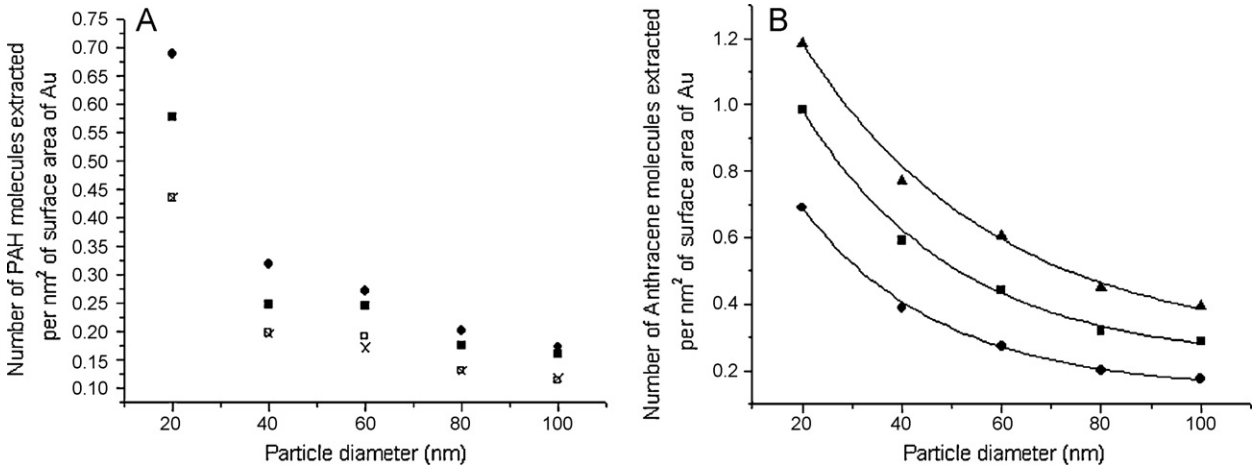

Fig. 2. (A) Number of PAH molecules extracted per nm^2 of surface area of Au as a function of particle diameter. Anthracene (●), pyerene (■), B[*a*]P (x) and indeno[*1,2,3-cd*]pyrene (□). Initial PAH concentration = 10 ng mL^{-1}. (B) Number of anthracene molecules extracted per nm^2 of surface area of Au as a function of particle diameter. Initial anthracene concentration = 10 ng mL^{-1} (●), 20 ng mL^{-1} (■) and 40 ng mL^{-1} (▲). The statistics of the fittings are the following: (●) $Y = 9.24X^{-0.86}$, $R = 0.9993$; (■) $Y = 10.08X^{-0.77}$; $R = 0.9973$; (▲) $Y = 9.34X^{-0.68}$; $R = 0.9964$.

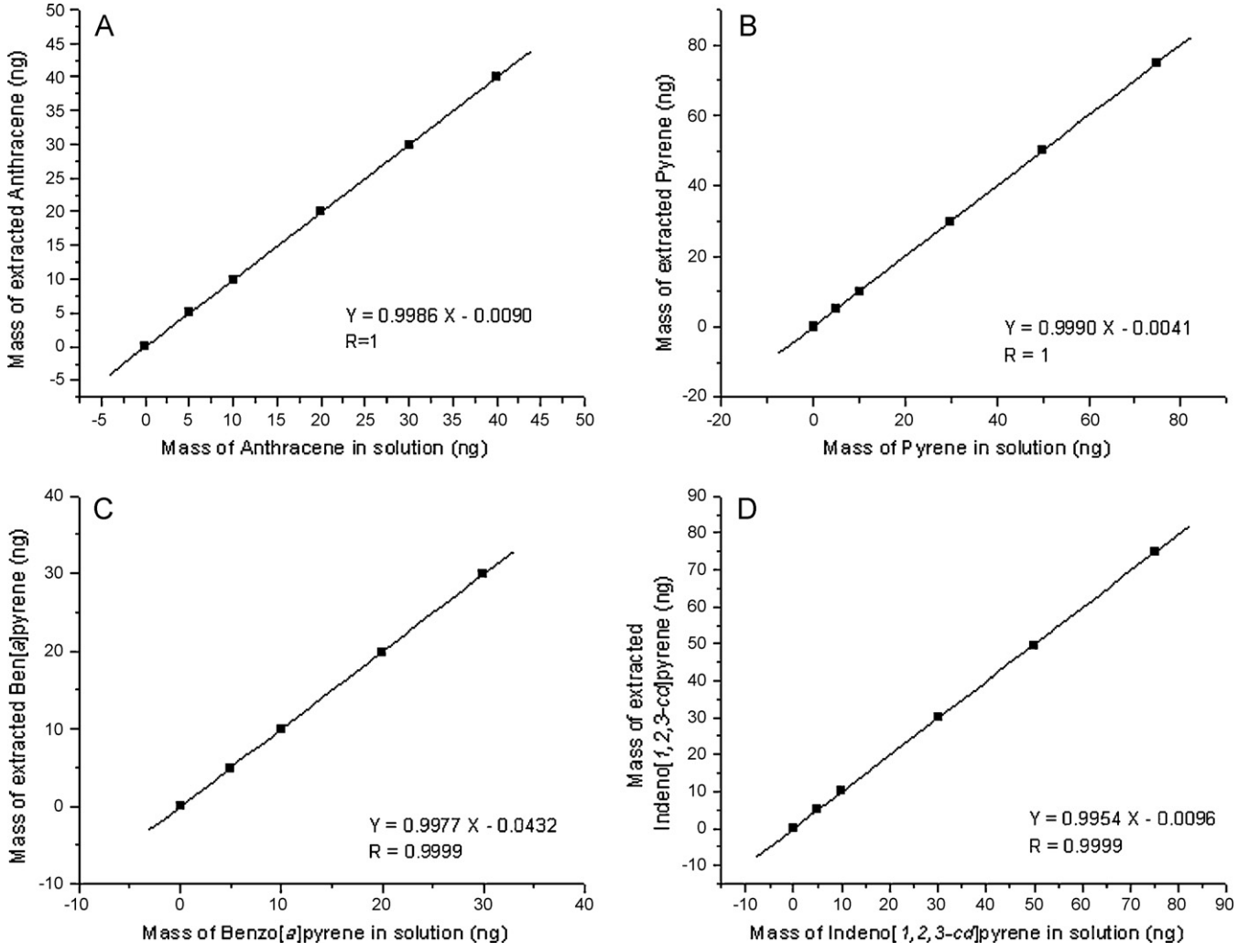

Fig. 3. Mass of extracted PAH as a function of its existing mass in solution. The statistics of the fittings were obtained via the least squares method.

3.3. Extraction with 20 nm Au NPs over a wide PAH concentration range

With the aim of providing sufficient surface area of Au to completely extract PAH at the working levels of Table 1, 0.95 mL of commercial Au NPs solution was used in the working solution. For the 20 nm particle diameter, this volume of colloid solution provides 8.356×10^{14} nm^2 of surface area, which is approximately 120 times larger than the one previously used (0.070×10^{14} nm^2). Stock solutions of anthracene, pyrene, B[*a*]P and indeno[*1,2,3-cd*]pyrene were prepared in methanol. 500 μL of PAH standard solution in 1% methanol–water (v/v) were added to the working solutions and shaken 5 min. The mixing, centrifugation and PAH monitoring were carried out as previously described. Fig. 3 shows the plots of "mass of extracted PAH" as a function of "mass of PAH in solution". The correlation coefficients (R) demonstrate excellent linear correlations between the extracted and the existing mass of PAH. The slopes very close to unity result from PAH extractions statistically equivalent to 100% ($\alpha = 0.05$, $N = 3$) over the entire working concentration ranges of the four PAH.

PAH concentrations in drinking water are usually below the lowest working concentrations in Table 1. The classical example is B[*a*]P, for which EPA has established a MCL of 0.2 ng mL^{-1} [3]. A suitable method for monitoring B[*a*]P in drinking water should then be able to determine its concentration at the parts-per-trillion (pg mL^{-1}) level. Arbitrarily, we set the maximum extractable concentration of our method as 2 ng mL^{-1} of B[*a*]P. Keeping in mind analysis cost, and considering that the previous surface area (8.356×10^{14} nm^2) would lead to unnecessary waste of Au, we carried out the following experiments: 500 μL of a 2 ng mL^{-1} B[*a*]P solution in 1% methanol–water (v/v) were mixed with 950 μL of extracting solutions containing 10, 50, 100 and 200 μL of 20 nm commercial Au NPs. Solution mixing, centrifugation and RTF measurements were performed as previously described. All extractions were carried out in triplicate. The solutions containing 10 and 50 μL Au NPs provided extraction efficiencies of 51.4 ± 1.2% and 98.7 ± 0.9%, respectively. The percents of extraction obtained with 100 and 200 μL Au NPs solutions were the same, i.e 99.6 ± 0.5%. Because this average is statistically equivalent to 100% ($P = 95\%$; $N = 3$) [30], all further studies were performed with 100 μL of 20 nm Au NPs solution.

3.4. Analysis of B[a]P by LETRSS

Previous studies in our group have shown that B[*a*]P in *n*-octane is a "two site system" [29]. The two orientations B[*a*]P molecules adopt in the frozen matrix produce two fluorescence spectra with the same vibronic structure but slightly shifted from one another. The two maximum wavelengths (λ_{em}) of the 0–0 transitions for the two sites appear at 403.10 ± 0.05 (site 1) and 403.20 ± 0.05 nm (site 2). These two sites are best observed at helium temperature, sample excitation at 368.2 nm and spectral band-pass equal or lower than 0.01 nm.

Fig. 4 reports the fluorescence spectrum recorded with the minimum (best) band-pass of the present instrument (0.1 nm), which was obviously insufficient to resolve the two crystallographic sites. The single peak that appeared at the 0–0 transition ($\lambda_{em} = 402.78 \pm 0.05$ nm) presented a single exponential decay with fluorescence lifetime (τ) equal to 37.90 ± 0.90 ns. This peak most likely reflected the predominant contribution of site 1 ($\lambda_{em} = 403.10$ nm; $\tau = 36.04 \pm 0.61$ ns) over site 2 ($\lambda_{em} = 403.20$ nm; $\tau = 45.68$ ns ± 0.84 ns). No attempts were made to improve instrumental resolution. The observed spectrum provided us with the spectral fingerprint to identify B[*a*]P in drinking water samples.

The forethought strategy to accomplish this task was to use an organic solvent with strong binding affinity for Au colloids.

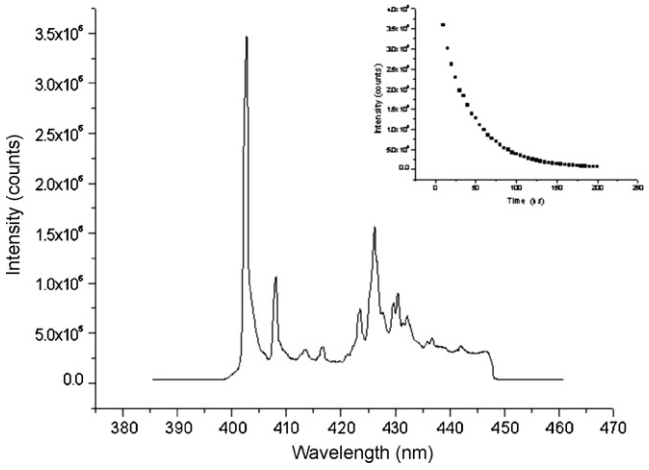

Fig. 4. 4.2K fluorescence spectrum and decay of a 2 ng mL^{-1} B[a]P solution in *n*-octane. Spectrum was recorded upon excitation at 298.0 nm using a 0.1 nm spectral band-pass. Delay and gate times were 10 and 150 ns, respectively. The following acquisition parameters were used for WTM (lifetime) collection: total gate time 200 ns, gate step = 5 ns, 100 laser pulses per spectrum.

Upon binding to the metallic surface, the organic solvent should release B[*a*]P to the surrounding solvent (*n*-octane) for LETRSS measurements. Several organic solvents were attempted, including *n*-octane, ethanol and methanol. The best results were obtained with 1-pentanethiol [22]. Because 1-pentanethiol was also found to be a strong quencher of B[*a*]P fluorescence, an optimization of its volume was then performed to completely release B[*a*]P at expenses of no fluorescence quenching. Volume optimization was carried out as follows: eight aliquots (500 μL each) of a water sample containing 2 ng mL^{-1} of B[*a*]P (1% methanol, v/v) were extracted in separate vessels with 950 μL of working solution contain 100 μL Au NPs 20 nm solution. Mixing and centrifugation were done as previously described. After removing the supernatant with a micro-pipette, each vessel was spiked with a different volume of 1-pentanethiol and brought to 100 μL with *n*-octane. After 5 min of equilibration time, the supernatants were transferred to the vessel of the cryogenic probe for 4.2K measurements at the maximum excitation and emission wavelengths of B[*a*]P.

Fig. 5 shows the signal intensity of B[*a*]P as a function of 1-pentanethiol volume. The highest fluorescence intensity was

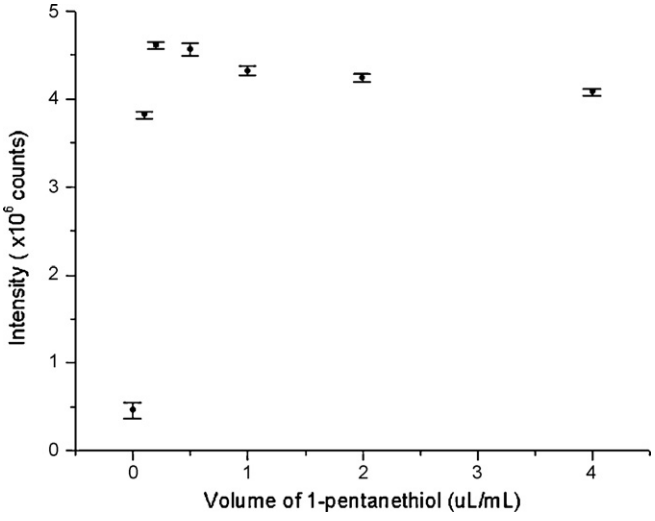

Fig. 5. 4.2K fluorescence intensity of B[*a*]P as a function of micro-litters (μL) of 1-pentanethiol. Each signal is the average of three individual measurements taken from three frozen aliquots. Relative standard deviations range between 1% and 5%.

Table 4
Analytical figures of merit for B[*a*]P.

Analytical figure of merit	LETRSS[a]	SPNE–LETRSS[b]
Linear dynamic range[c] (ng mL^{-1})	0.05–2	0.004–2
Correlation coefficient	0.9990	0.9996
Limit of detection (ng mL^{-1})	0.02	0.001
Absolute limit of detection[d] (ng)	0.002	0.0005
Relative standard deviations[e] (%)	10–0.2	7.3–0.2

[a] B[*a*]P solutions were prepared in n-octane. 4.2K fluorescence was measured at the maximum excitation (298.0 nm) and emission (402.7 nm) wavelengths.
[b] Measuring parameters for LETRSS were the same as ([a]).
[c] Lowest concentration of linear dynamic range corresponds to the limit of quantitation.
[d] Absolute limit of detection was calculated as follows: [sample volume] × [limit of detection].
[e] Relative standard deviations report the values obtained with concentrations equivalent to the limits of quantitation and the upper concentration limits of the calibration curves.

observed upon complete release of B[*a*]P, which occurred at 0.2 μL of 1-pentanethiol. Beyond this point, the concentration of B[*a*]P in the supernatant (*n*-octane) should then remain constant for the rest of the titration. The same should be true for its fluorescence intensity unless quenching occurred. The signal intensity at 0.5 μL of 1-pentanethiol was statistically equivalent ($P = 95\%$; $N_1 = N_2 = 3$) [30] to the one at 0.2 μL. The excess of 1-pentanethiol caused no fluorescence quenching because it probably bonded to free surface of Au still available for interaction. The degree of fluorescence quenching progressed as the volume of 1-pentanethiol increased from 1 to 4 μL of solvent. The observed trend is here attributed to the excess of unbound 1-pentanethiol that went into the octane layer and interacted with B[*a*]P.

The fluorescence lifetimes recorded from the 100 μL of supernatants support our assumptions. From 0.1 to 0.5 μL of 1-pentanethiol, the τ values were statistically equivalent to the lifetime of the supernatant in the absence of 1-pentanethiol ($\tau = 37.7 \pm 0.4$ ns; $N = 3$). Within this volume range, all the lifetimes were statistically equivalent to the lifetime of B[*a*]P in pure *n*-octane (37.90 ± 0.90 ns). This is a strong indication that 1-pentanethiol complete bonded to the surface of Au and it remained adsorbed on the metallic surface. After adding 1 μL of 1-pentanethiol, the lifetime of the supernatant dropped to a statistically lower value ($\tau = 35.2 \pm 0.6$ ns; $\alpha = 0.05$; $N_1 = N_2 = 3$) [30], denoting the presence of 1-pentanethiol in the layer of *n*-octane. As the addition of 1-pentanethiol progressed, the fluorescence lifetime of the supernatant became even shorter and reached its minimum value (34.0 ± 0.5 ns) at 4 μL of 1-pentanethiol. All further studies were then performed with 0.2 μL of 1-pentanethiol.

Table 4 compares the analytical figures of merit of B[*a*]P obtained via LETRSS and SPNE-LETRSS. The linear dynamic ranges are based on the average intensities of at least five PAH concentrations. Each average was calculated from a minimum of three individual measurements taken from three frozen aliquots. The upper concentration (2 ng mL^{-1}) is the same for both methods and corresponds to the maximum extractable concentration we arbitrarily set for SPNE. The limit of quantitation (LOQ) and the limit of detection (LOD) were calculated as $10\,S_B/m$ and $3\,S_B/m$, respectively. S_B was the standard deviation from 16 blank determinations and m was the slope of the calibration curve. The excellent reproducibility provided outstanding precision of measurements at the parts-per-trillion (pg mL^{-1}) concentration level. For a 500 μL sample volume, the absolute LOD via SPNE-LETRSS was at the femtogram level (50×10^{-15} g). This detection limit is equivalent to 182×10^{-18} mols of B[*a*]P. To the extent of our literature search, there are no methods capable to detect attomol levels of B[*a*]P in micro-litters of water sample.

3.5. Direct analysis of B[a]P in tap water samples

Because B[*a*] is the only PAH for which EPA has set a MCL in community water systems, we found it appropriate to test the recovery of our approach with tap water samples. Tap water was spiked with μL volumes of stock solutions in methanol to provide final concentrations of B[*a*]P equal to 0.05, 0.1 and 0.2 ng mL^{-1}. Each water sample was examined in triplicate. Quantitative analysis was made via the calibration curve method. The average recoveries were 87.5% for 0.05 ng mL^{-1}, 98.6% for 0.1 ng mL^{-1} and 96.5% for0.2 ng mL^{-1}. Spectral purity, i.e. the absence of matrix interference, was further confirmed via fluorescence decay analysis at the maximum excitation and emission wavelengths of B[*a*]P. Single exponential decays with fluorescence lifetime values equivalent to the lifetime of the pure compound in *n*-octane ($\tau = 37.90$ ns) were obtained in all cases.

4. Conclusion

Within the 20–100 nm particle diameter range, the 20 nm Au NPs showed the best extraction efficiencies. Independent of the size of the PAH (3, 4 and 5 rings), 20 nm Au NPs were able to extract more PAH molecules per nm^2 of surface area of Au than the larger particles. The complete extraction of PAH requires the availability of sufficient surface area of Au for PAH adsorption. For 20 nm Au NPs, a 8.356×10^{14} nm^2 surface area of Au was sufficient to completely extract PAH at their highest working concentrations, which ranged from 30 ng mL^{-1} (B[*a*]P and indeno[*1,2,3-cd*]pyrene]) to 75 ng mL^{-1} (pyrene). These concentrations are much higher than the PAH levels usually found in water samples. A 100 μL of 20 nm commercial Au NPs solution was sufficient to completely extract 2 ng mL^{-1} of B[*a*]P in drinking water. This concentration is 10× higher than the EPA MCL for B[*a*]P.

The complete release of B[*a*]P into the Shpol'skii matrix (*n*-octane) was best accomplished with 0.2 μL 1-pentanethiol, a solvent with strong chemical affinity for Au colloids. The migration of B[*a*]P into the layer of *n*-octane provides a highly resolved spectrum with a distinct fluorescence lifetime. The pre-concentration achieved with SPNE improved the LOD of LETRSS by an order of magnitude. The improvement reflected the higher sensitivity of SPNE-LETRSS over LETRSS. For a 500 μL sample volume, the absolute LOD was at the picogram concentration level (0.5×10^{-12} g) or femtomol (1.8×10^{-15}) level. To the extent of our literature search, there are no methods capable to detect these levels of PAH in micro-litters of water sample. The excellent reproducibility provided outstanding precision of measurements at the parts-per-trillion (pg mL^{-1}) level.

When combined to LETRSS, the new method is environmentally friendly and cost effective. The entire procedure only consumes 100 μL of organic solvents and 100 μL of 20 nm Au NPs per sample. The extraction procedure is well suited for routine analysis of numerous samples as the small working volume facilitates the implementation of simultaneous sample extraction. With the aid of the cryogenic probe, LETRSS measurements are straightforward and take less than 10 min/sample.

References

[1] Polycyclic Aromatic Hydrocarbons: 15 Listings, U.S. Department of Health and Human Services, Ninth Report on Carcinogens. http://ehp.niehs.nih.gov/roc/ninth/rahc/pahs.pdf, 2001.
[2] Methods for the Determination of Organic Compounds in Drinking Water, EPA 600/4-88/039, U.S. Government Printing Office, Washington, DC, 1991.
[3] US EPA, http://www.epa.gov/safewater/standards.html.
[4] W.D. Wang, Y.M. Huang, W.Q. Shu, J. Cao, J. Chromatogr. A 27 (2007) 1173.
[5] P. Oleszczuk, S. Baran, J. Hazard. Mater. B 113 (2004) 237.
[6] G. Kiss, Z. Varga-Puchony, J. Hlavay, J. Chromatogr. A 725 (1996) 261.
[7] I. Urbe, J. Ruana, J. Chromatogr. A 778 (1997) 337.

[8] L. Bernal, M.J. Nozal, L. Toribio, M.L. Serna, F. Borrull, R.M. Marce, E. Pocurull, J. Chromatogr. A 778 (1997) 321.
[9] W. Kanchanamayoon, N. Tatrahun, World J. Chem. 3 (2008) 51.
[10] S.R. Sargenti, H.M. McNair, J. Microcolumn Sep. 10 (1998) 125.
[11] G. Carrera, P. Fernandez, R. Vilanova, J.O. Grimalt, J. Chromatogr. A 823 (1998) 189.
[12] N.Q. Li, H.K. Lee, J. Chromatogr. A 921 (2001) 255.
[13] K. Li, H.F. Li, L.B. Liu, Y. Hashi, T. Maedac, J.M. Lin, J. Chromatogr. A 1154 (2007) 74.
[14] A.D. Campiglia, A.J. Bystol, S. Yu, Anal. Chem. 78 (2006) 484.
[15] A.D. Campiglia, S. Yu, A.J. Bystol, H. Wang, Anal. Chem. 79 (2007) 1682.
[16] C. Gooijer, F. Ariese, J.W. Hofstraat, Shpol'skii spectroscopy and other-site selection methods: applications in environmental analysis, bioanalytical chemistry; and chemical physics, in: J.D. Winefordner (Ed.), Chemical Analysis: A Series of Monographs on Analytical Chemistry and Its Applications, vol. 156, Wiley-Interscience, New York, 2000.
[17] S. Yu, A.D. Campiglia, Appl. Spectrosc. 58 (2004) 1385.
[18] S. Yu, A.D. Campiglia, Anal. Chem. 77 (2005) 1440.
[19] A.J. Bystol, T. Thorstenson, A.D. Campiglia, Environ. Sci. Technol. 36 (2002) 4424.
[20] A.J. Bystol, S. Yu, A.D. Campiglia, Talanta 60 (2003) 449.
[21] A.F. Arruda, S. Yu, A.D. Campiglia, Talanta 59 (2003) 1199.
[22] H. Wang, A.D. Campiglia, Anal. Chem. 80 (2008) 8202.
[23] H. Wang, S. Yu, A.D. Campiglia, Anal. Chem. 385 (2009) 249.
[24] H. Wang, W.B. Wilson, A.D. Campiglia, J. Chromatogr. A 385 (2009) 249.
[25] A.J. King, J.W. Readman, J.L. Zhou, Anal. Chim. Acta 523 (2004) 267.
[26] R. Barra, P. Popp, R. Quiroz, C. Bauer, H. Cid, W. von, Tumpling, Chemosphere 58 (2005) 905.
[27] M.A. Olivella, Chemosphere 63 (2006) 116.
[28] A.J. Bystol, A.D. Campiglia, G.D. Gillispie, Appl. Spectrosc. 54 (2000) 910.
[29] A.J. Bystol, A.D. Campiglia, G.D. Gillispie, Anal. Chem. 73 (2001) 5762.
[30] M.J. Miller, J.C. Miller, Statistics and Chemometrics for Analytical Chemistry;, 4th Ed., Prentice-Hall, Inc., 2000.